Simultaneous measurements of unstable and stable Alfvén Eigenmodes in JET

R.A. Tinguely[1]‡, J. Gonzalez-Martin[2], P.G. Puglia[3], N. Fil[4], S. Dowson[4], M. Porkolab[1], I. Kumar[5], M. Podestà[6], M. Baruzzo[4], A. Fasoli[3], Ye.O. Kazakov[7], M.F.F. Nave[8], M. Nocente[9] [10], J. Ongena[7], Ž. Štancar[11], and JET Contributors*

[1] Plasma Science and Fusion Center, Massachusetts Institute of Technology, Cambridge, MA, USA

[2] Department of Physics and Astronomy, University of California, Irvine, California 92697, USA

[3] Ecole Polytechnique Fédérale de Lausanne (EPFL), Swiss Plasma Center (SPC), CH-1015 Lausanne, Switzerland

[4] Culham Centre for Fusion Energy, Culham Science Centre, Abingdon, UK

[5] Durham University, Durham, UK

[6] Princeton Plasma Physics Laboratory, Princeton, NJ, USA

[7] Laboratory for Plasma Physics, LPP-ERM/KMS, TEC Partner, 1000 Brussels, Belgium

[8] Instituto de Plasmas e Fusão Nuclear, Instituto Superior Técnico, Univ. de Lisboa, Lisbon, Portugal

[9] Dipartimento di Fisica, Universitá di Milano-Bicocca, 20126 Milan, Italy

[10] Institute for Plasma Science and Technology, National Research Council, 20125, Milan, Italy

[11] Jožef Stefan Institute, Ljubljana, Slovenia

* See author list of J. Mailloux *et al* 2022 *Nucl. Fusion*, doi:10.1088/1741-4326/ac47b4

Abstract. In this paper, we report the novel experimental observation of both unstable and stable Toroidicity-induced Alfvén Eigenmodes (TAEs) measured simultaneously in a JET tokamak plasma. The three-ion-heating scheme (D-DNBI-^{3}He) is employed to accelerate deuterons to MeV energies, thereby destabilizing TAEs with toroidal mode numbers $n = 3{-}5$, each decreasing in mode amplitude. At the same time, the Alfvén Eigenmode Active Diagnostic resonantly excites a stable $n = 6$ TAE with total normalized damping rate $-\gamma/\omega_0 \approx 1\%{-}4\%$. Hybrid kinetic-MHD modeling with codes NOVA-K and MEGA both find eigenmodes with similar frequencies, mode structures, and radial locations as in experiment. NOVA-K demonstrates good agreement with the $n = 3$, 4, and 6 TAEs, matching the damping rate of the $n = 6$ mode within uncertainties and identifying radiative damping as the dominant contribution. Improved agreement is found with MEGA for *all* modes: the unstable $n = 3{-}5$ and stable $n = 2, 6$ modes, with the latter two stabilized by higher intrinsic damping and lower fast ion drive, respectively. While some discrepancies remain to be resolved, this unique validation effort gives us confidence in TAE stability predictions for future fusion devices.

‡ Author to whom correspondence should be addressed: rating@mit.edu

Keywords: Alfvén Eigenmodes, stability, three-ion-heating, Ion Cyclotron Resonance Heating, Neutral Beam Injection

1. Introduction

Alfvén Eigenmodes (AEs), destabilized by fast ions (FIs) in tokamak plasmas, have been the subject of intense investigation due to their potential to enhance the transport and thus degrade the confinement of said FIs [1]. This should be avoided in future fusion devices, like ITER and SPARC, which aim to maximize confinement and fusion power.

Unstable AEs are often easily observable in high-frequency fluctuation data, e.g. from passive magnetic probes, interferometry, reflectometry, soft x-ray (SXR), and other signals. However, the measurement of *stable* AEs requires a system like JET's Alfvén Eigenmode Active Diagnostic (AEAD) [2], comprising two in-vessel, toroidal arrays of four antennas each [3]. The antennas are independently powered and phased by amplifiers with currents up to ∼10 A, frequencies ranging 25−250 kHz, and a toroidal mode number spectrum $|n| < 20$ [4]. When the AEAD's frequency scan intersects the resonant frequency $\omega_0 = 2\pi f_0$ [rad s^{-1}] of a stable§ AE, the plasma responds like a weakly damped, driven harmonic oscillator; the damping rate γ [s^{-1}] and n-number are then deduced from the magnetic response measured by up to fourteen fast magnetic probes [5].

Many past studies have analyzed unstable AEs and compared with modeling efforts (see [6, 7] and references therein). It has been found [8] that many codes can identify the same AE and calculate similar contributions of *drive* to the total growth rate. However, the evaluation of the contribution from *damping* is more variable. Therefore, much work has gone into the analysis of stable AEs and their net damping rates, in both JET [2, 9–11] (and references therein) and Alcator C-Mod [12–14]. Still, there can be a disconnect of sorts between un/stable AEs if they are not measured under the same plasma conditions.

In this paper, we report (for the first time, to the authors' knowledge) the *simultaneous* measurements of three destabilized Toroidicity-induced Alfvén Eigenmodes (TAEs) and one stabilized TAE in a JET deuterium plasma discharge. Experimental values of the net growth rates, frequencies, and mode numbers and locations allow direct comparison with AE stability codes. Agreement between experiment and models gives us greater confidence in the prediction of AE stability for future devices; in particular, complementary analyses from the recent JET DT campaign [15] will identify and validate the contribution of alphas to AE drive.

We note here that such a measurement of concurrent unstable and stable AEs can be difficult to achieve in JET: First, the AEAD perturbation only resonates with a stable AE if their frequencies match and the mode location is accessible. Then, the fast magnetics only measure the resonance if the signal is sufficiently strong and the damping rate not too large. In JET, the magnetic field strength is typically too high for FIs from Neutral Beam Injection

§ Note that the AEAD *can* interact with unstable AEs, but for sufficiently destabilized mode amplitudes, the growth rate cannot be straightforwardly determined from the response.

(NBI) to drive AEs unstable; thus, AEs are usually only destabilized during Ion Cyclotron Resonance Heating (ICRH). However, the AEAD is not efficient during H-mode [11], so the AEAD measures only few stable AEs during ICRH (and NBI), regardless of unstable AEs being observed at the same time.

The outline of the rest of the paper is as follows: In Section 2, the experimental measurements of both stable and unstable AEs are presented. Sections 3 and 4 then show simulation results from hybrid kinetic-MHD codes NOVA-K [16–18] and MEGA [19], respectively. Finally, a discussion and summary is given in Section 5.

2. Experimental measurements of AE stability

In this section, we report the novel experimental observation of stable and unstable AEs *simultaneously* measured in JPN 94700. This pulse is part of the three-ion-heating scenario development experiments at JET [20]; in fact, extensive analyses of the following, similar plasma discharge, JPN 94701, are reported in [21]. Experimental results are presented here, and further kinetic-MHD simulations with NOVA-K [16–18] and MEGA [19] are given in Sections 3 and 4, respectively.

The time evolution of plasma parameters for JPN 94700 are shown in Fig. 1a. During the time range of interest, $t = 7.5{-}11$ s (shaded), steady-state plasma parameters are $B_0 = 3.7$ T, $I_\mathrm{p} = 2.5$ MA, $n_\mathrm{e0} = 6 \times 10^{19}$ m^{-3}, and $T_\mathrm{e0} = 5.5{-}7$ keV, although note the large sawtooth crashes at $t \approx 8$ s and 8.8 s. Auxiliary heating powers are Neutral Beam Injection (NBI) of $P_\mathrm{NBI} = 6$ MW, with ∼300 ms "blips" up to 8 MW at $t \approx 9$ s and 9.6 s, and Ion Cyclotron Resonance Heating (ICRH) of $P_\mathrm{ICRH} = 4$ MW stepping up to 6 MW at $t \approx 8.5$ s. The concentration of ^{3}He is $n_\mathrm{He3}/n_\mathrm{e} \approx 27\%$ as part of the D-(DNBI)-^{3}He heating scenario [21].

Profiles of various plasma parameters are shown in Fig. 1b for one time of interest, $t = 9.9$ s. The electron density and temperature profiles, from Thomson scattering, match the fitted profiles from TRANSP [23–25] well. Note here that an effective ion density profile, including the relatively high concentration of ^{3}He, is used in the simulations of the following sections. The rotation profile is obtained from ^{3}He charge exchange spectroscopy.

The safety factor profile is solved iteratively with EFIT [22], including constraints from kinetic pressure and additionally polarimetry; both q-profiles are similar in Fig. 1b. It is important to note here that this can be one of the largest sources of uncertainty in the analysis below. The observation of Reverse Shear AEs (RSAEs), or Alfvén Cascades, starting at $t \approx 8.9$ s (see Fig. 2) indicates that a non-monotonic q-profile exists for some time period following the sawtooth crash at $t \approx 8.8$ s. Further constraints from Motional Stark Effect data have been used to identify reverse shear in similar plasmas [26]; however, such data were unfortunately not available for this pulse. That said, the upward-chirping RSAEs attain their maximum frequencies around $t \approx 9.9$ s, meaning that relaxation to a monotonic q-profile is plausible by this time. A central safety factor $q_0 \approx 0.8$ is consistent with the previously sawtoothing profile, but with fast ion stabilization. As will be shown, good agreement between experiment and modeling is attained with the q-profile shown in Fig. 1b.

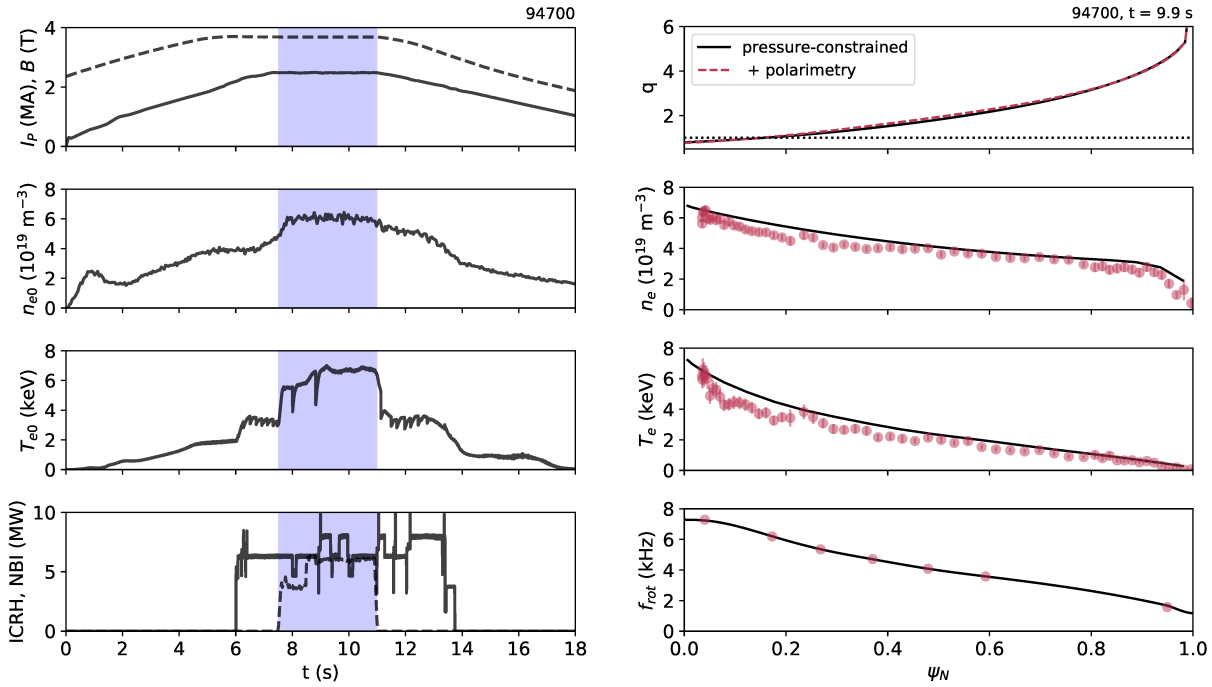

(a) (b)

Figure 1: (a) Plasma parameters for JPN 94700: toroidal magnetic field (dashed), plasma current (solid), central electron density from Thomson Scattering (TS) and temperature from Electron Cyclotron Emission, and heating powers from NBI (solid) and ICRH (dashed). Both stable and unstable AEs were measured during the shaded time interval. (b) Profiles at $t = 9.9$ s: safety factor from EFIT [22] constrained by pressure only (solid) and additionally polarimetry (dashed) with $q = 1$ dotted, electron density and temperature from TS, and rotation frequency from ^{3}He charge exchange. Experimental data are shown as circles with uncertainties as error bars, while solid lines are fits to the data.

TAEs are destabilized by the FI population during $t = 7.5{-}11$ s, as seen in the spectrogram of Fig. 2a. This is the Fourier decomposition of magnetic fluctuation data in both time and toroidal angle; thus, we can clearly identify coherent TAEs in time, frequency, and with a specific n-value. At first ($t \approx 7.5{-}8$ s and $P_{\mathrm{ICRH}} = 4$ MW), only $n = 2, 3$ TAEs are driven unstable, and then the modes quickly disappear with the sawtooth crash at $t \approx 8$ s. This is likely due to the changing q-profile and/or redistribution of FIs.

As ICRH increases to $P_{\mathrm{ICRH}} = 6$ MW, $n = 2{-}4$ TAEs are destabilized from $t \approx 8.3{-}8.8$ s, again stabilizing with the sawtooth crash at $t \approx 8.8$ s. From $t \approx 9{-}11$ s, the FIs destabilize $n = 3 - 5$ TAEs and stabilize the sawteeth; interestingly, note that the $n = 2$ mode has now stabilized. The $n = 1$ and 6 TAEs are also not observed in the spectrogram during this time interval at all. Furthermore, the frequency-spacing between mode numbers is $\Delta f \approx 10{-}20$ kHz, which is slightly larger than the on-axis rotation frequency (see Fig. 1b); the additional shift could be explained by different mode locations within the TAE gap.

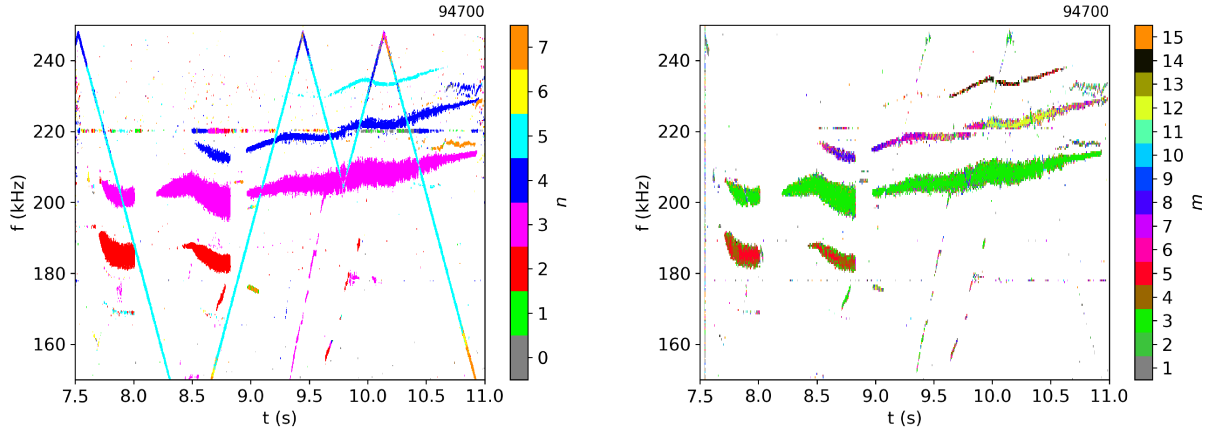

(a) (b)

Figure 2: Fourier decomposition of magnetics data with (a) toroidal and (b) poloidal mode number analysis for JPN 94700. Note that AEAD signals and ICRH beat frequencies have been (almost) subtracted from the background in (b).

From the magnetics data, the amplitudes of the $n = 3{-}5$ modes decrease by approximately an order of magnitude with each increasing n, and this is qualitatively seen in the spectrograms of Fig. 2. However, deducing true mode amplitudes with edge diagnostics is difficult, especially with fields decreasing approximately as $\propto r^{-m}$. That said, the $n = 2, 3$ TAEs are also observed as low-amplitude fluctuations in the SXR array, localizing them approximately within $q \sim 2$;‖ $n = 4, 5$ TAEs are not seen in the SXR data, likely due to a too low signal-to-noise ratio.

Throughout this discharge, the AEAD scans in frequency, sometimes resonantly exciting stable AEs. This scan can be seen in Fig. 2a as the triangular waveform. Interestingly, the predominant mode number identified by the magnetic probes for the AEAD perturbation is $n = 5$, although all antennas have the same phase; therefore, power *should* be injected into a spectrum of mode numbers peaked around $n = 0$, with a higher likelihood of exciting even than odd n-numbers.

A poloidal mode number (m) analysis is also performed, with the resulting spectrogram shown in Fig. 2b. As with the n-calculation, this is a chi-square minimization of the phase difference between probes, iterating over all probes as the reference [5]. We calculate the poloidal angle of each probe with respect to the magnetic axis from EFIT, but ignore the mode location in the evaluation. We additionally include an inverse variance weighting, assuming that the standard deviation is the distance from the poloidal probe position to the magnetic axis. Furthermore, we restrict the poloidal harmonic range to $m \in [n, 3n]$, assuming the mode is located within $q \leq 3$ for computational efficiency. This assumption is valid for this analysis, as will be shown in the next sections, but is an overall limitation; thus, there

‖ Reflectometry data were not available for the pulse of interest, JPN 94700; however, those data from a similar discharge, JPN 95683, localized similar TAEs just outside $q \sim 1$ [21].

could be possible effects from aliasing.

While there are certainly larger uncertainties associated with this m-calculation, the results align with expectations: a mix of $m = 4, 5$ (brown, red) is seen for the $n = 2$ TAE, and $m = 3$ (green) dominates for $n = 3$; these are then located within $q < 5/2$, agreeing approximately with the SXR data. Many m-numbers appear for both $n = 4$ and 5, but $m = 12$ (yellow) and 14 (orange), respectively, might stand out as the clearest poloidal harmonics; this suggests localizations closer to $q \sim 3$, although they could not be identified in the SXR signal. Finally, note that both the AEAD and ICRH beat frequencies are (almost) subtracted from the background of this spectrogram; this was done only as part of a larger database analysis of unstable TAEs in JET.

The AEAD frequency scan is reproduced in Fig. 3; here, the amplitude of the magnetic response (summed over all probes) is also shown, and two pairs of broad peaks are visible around $t \approx 9.5$ s and 10.1 s. These are identified as four measurements of the same stable AE resonance, with resonant frequency $f_0 \approx 245$ kHz. This is higher than the unstable $n = 5$ TAE in Fig. 2a, indicating that it could be a Doppler-shifted $n = 6$ TAE. Unfortunately, this mode could only be measured by a few magnetic probes; the limited number of probes and their toroidal separation did not enable a reliable determination of the mode's toroidal mode number. The (normalized) damping rate measurements range from $-\gamma/\omega_0 \approx 2{-}3\%$, with relatively large uncertainties $\Delta(\gamma/\omega_0) \approx \pm 1\%$.¶ A stable $n = 6$ mode is expected since the $n = 5$ mode is low amplitude and could be only marginally unstable, i.e. $\gamma/\omega_0 \sim 0$.

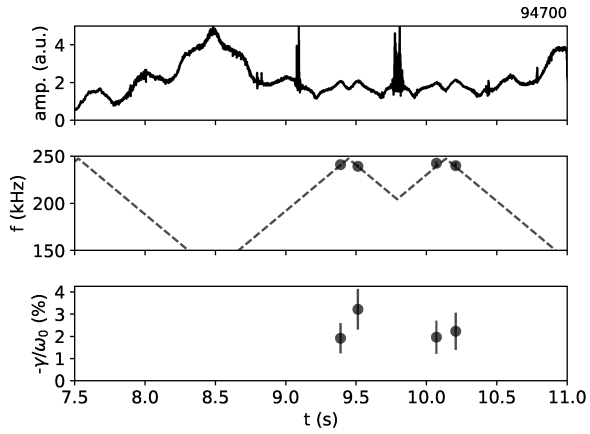

Figure 3: Stable AE resonance measurements: the magnetic response amplitude (summed over all probes), AEAD (dashed) and resonant frequencies (circles), and normalized damping rates with uncertainties as error bars.

The deuterium FI distribution function is calculated from TRANSP [23–25], using the NUBEAM [27] and TORIC [28] modules, and is shown in Fig. 4 as a function of radius, energy, and pitch. The NBI population is seen with a birth energy ∼100 keV, and the

¶ Note that γ has units s^{-1}, and ω_0 has units $\mathrm{rad\,s}^{-1}$ and not Hz.

ICRH-accelerated tail extends to energies ∼2.5 MeV with a dominant volume-averaged pitch $v_\parallel/v \approx 0.5$. As will be discussed in the following sections, analytic fits of the FI distribution function are performed for both NOVA-K and MEGA simulations.

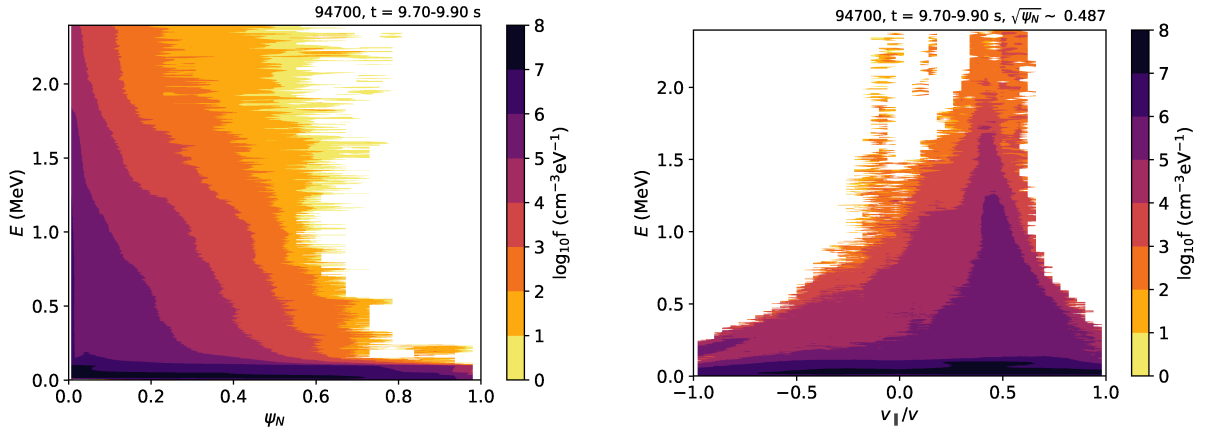

(a) (b)

Figure 4: Deuterium FI distribution functions (logarithmic) from TRANSP for JPN 94700 and integrated over $t = 9.7{-}9.9$ s: (a) averaged over all pitches, and (b) at $\sqrt{\psi_N} \approx 0.5$.

3. Kinetic-MHD simulations with NOVA-K

The kinetic-MHD code NOVA-K [16–18] is used to identify AEs and assess their stability at one time, $t = 9.9$ s. This time is selected because it occurs during a relatively steady-state period of the pulse (see Fig. 1a), i.e. after sawtooth stabilization, and in between the measurements of stable AEs by the AEAD (see Fig. 3). The plasma profiles (see Fig. 1b) are used in the calculation of the Alfvén continua and eigenmode structures for $n = 2{-}6$, with a subset shown in Fig. 5. Note that the TAE eigenfrequencies are in the *lab* frame, as the experimental rotation profile is included in NOVA-K; they span $f \approx 195{-}225$ kHz (see Table 1), which is only slightly lower than those observed experimentally (see Fig. 2). This ∼10% difference is likely the result of uncertainties in the density, safety factor, and rotation profiles; the adiabatic index used in NOVA-K could also play a role [29].

The poloidal mode structures from NOVA-K for each n (see Fig. 5) are primarily dominated by harmonics $m = n, n+1$, i.e. localizing the TAEs around $q \approx 1$ and consistent with the SXR data, although the overall structures are quite global. From the NOVA-K results, we may have expected $m = 4$ to be identified as the dominant poloidal harmonic for the $n = 3$ TAE in Fig. 2b, but instead $m = 3$ is found experimentally. Similarly, the higher poloidal harmonics $m = 12$ and 14 for $n = 4$ and 5 TAEs, respectively, are not dominant in NOVA-K, but perhaps their closer location to the poloidal probes increases their detection probability in experiment. For example, see the $m = 14$ harmonic for the $n = 5$ TAE in Fig. 5c. Unfortunately, the SXR array can help localize these modes, identified by frequency,

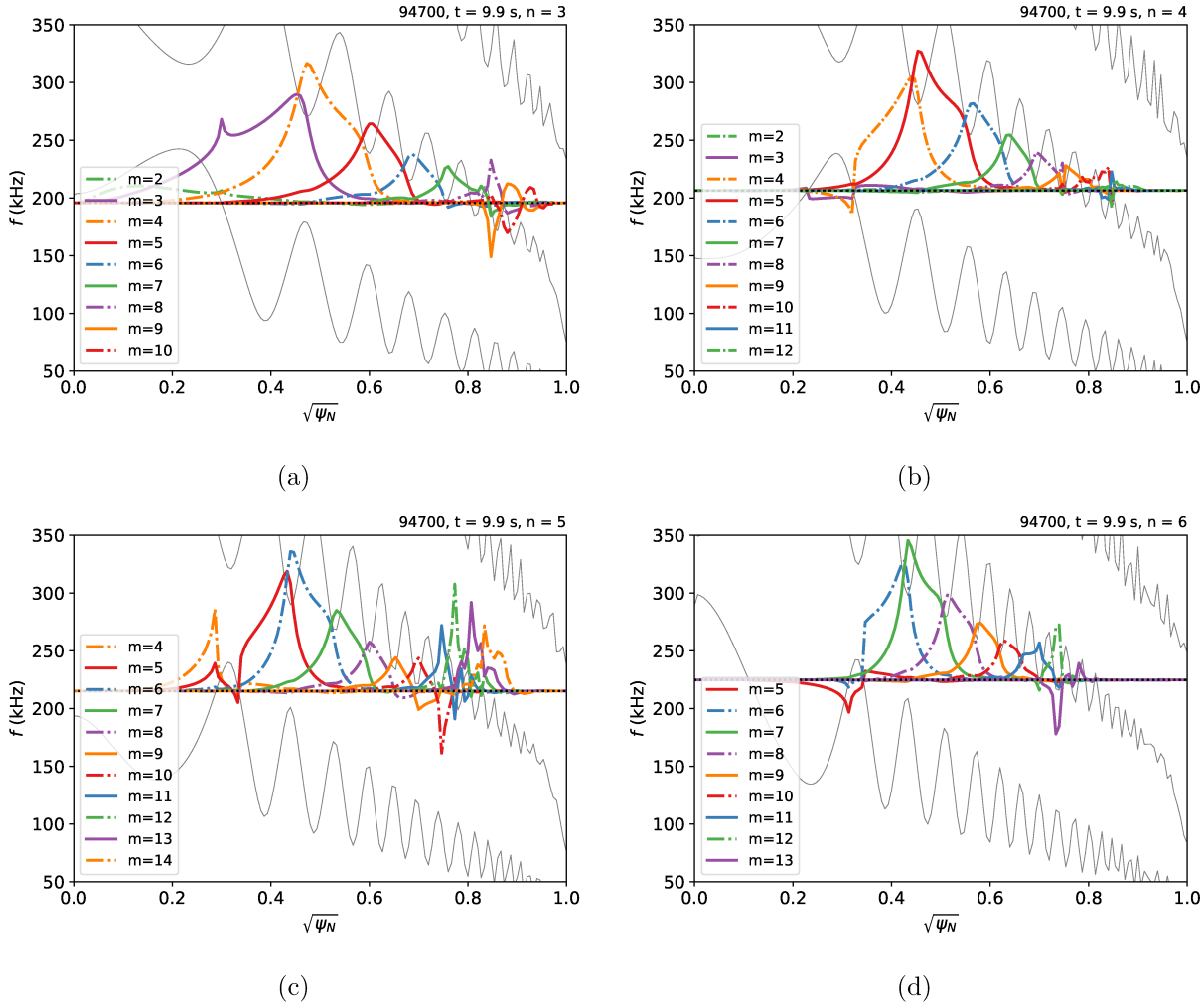

Figure 5: Continua (thin lines) and poloidal mode structure (solid, dot-dashed) from NOVA-K at $t = 9.9$ s for $n =$ (a) 3, (b) 4, (c) 5, (d) 6. The frequency (lab-frame) is indicated by the horizontal dotted line. ψ_N is the normalized poloidal flux. While the ranges of poloidal harmonics (m) vary for each subplot, the colors and line styles are the same for all.

but their low signals and measurement by only a few SXR lines-of-sight make a mode number evaluation infeasible. This demonstrates the difficulty of measuring some properties of core modes from edge diagnostics.

The stability of the $n = 2{-}6$ TAEs is computed including the effects of the FIs. In NOVA-K, an energy threshold[+] is used to discriminate the NBI and ICRH populations within the FI distribution function from TRANSP and NUBEAM, which is important here because this three-ion-heating scenario specifically heats the DNBI ions. Then, for each radial position, the local NBI population is fit with an anisotropic slowing down distribution, while the ICRH tail is fit with an anisotropic equivalent temperature [13]. Furthermore, the ICRH

[+] Note that the threshold was varied among 125 keV, 150 keV, and 200 keV with little impact on the stability results.

resonance layer is modeled as a Gaussian profile, in this case with its peak at the magnetic axis ($R_0 \approx 3$ m) and width $\Delta R \approx 0.24$ m, similar to that shown in [21] (see Fig. 12a therein).

The breakdown of various drive and damping mechanisms is given in Table 1. Radiative damping is the largest contribution; this has also been identified in other recent analyses of (asynchronous) unstable [30, 31] and stable [10, 11] AEs in JET. While the implementation of radiative damping, which is averaged over the radial mode structure in NOVA-K, comes from [32, 33], Ref. [34] can help us estimate the *relative* uncertainty: $\Delta(\gamma/\omega_0)_{\rm rad} \propto (1/3)(\gamma/\omega_0)_{\rm rad}\,(\mathrm{d}\ln T + \mathrm{d}\ln q)$, which is $\sim$8% assuming 10% uncertainties in the plasma profiles. Continuum damping can also be a significant contributor, which is clear from the eigenmodes' intersecting the continuum around $\sqrt{\psi_{\rm N}} \approx 0.8$ in Fig. 5, although absolute uncertainties can be of order $\Delta(\gamma/\omega_0) \sim 0.1\%$ [35].

Table 1: Growth rates (%, damping < 0) calculated from NOVA-K. The frequency is in the lab frame; the *absolute* uncertainty in continuum damping is $\pm 0.1\%$, while the *relative* uncertainty in radiative damping is $\pm 8\%$. Totals are given **with** and *without* the contributions from fast ions, which include finite Larmor radius effects.

Toroidal mode number (n)	2	3	4	5	6
Frequency (kHz, lab frame)	179.9	195.9	206.5	215.1	224.7
Damping/drive mechanism	Growth rate γ/ω_0 (%)				
Continuum	-0.06	-0.03	-0.77	-0.33	-0.31
Radiative	-1.03	-2.01	-2.84	-4.44	-4.76
Electron collisional	-0.32	-0.39	-0.04	-0.04	-0.01
Electron Landau	-0.09	-0.11	-0.07	-0.12	-0.12
Ion Landau	-0.02	-0.01	-0.04	-0.01	-0.01
NBI fast ions	-0.07	-0.12	-0.11	$\sim$0	-0.05
ICRH fast ions	4.08	4.30	4.45	2.01	2.34
Total (w/o fast ions)	*-1.53*	*-2.54*	*-3.76*	*-4.94*	*-5.22*
Total (w/ fast ions)	**2.48**	**1.64**	**0.58**	**-2.93**	**-2.92**

Due to the high magnetic field (and thus high Alfvén speed), NBI ions actually Landau damp these modes in JET [36], but ICRH FIs provide significant drive, $\gamma/\omega_0 \approx 2$–$4\%$. Thus, $n = 2$–4 TAEs are predicted by NOVA-K to be destabilized, with decreasing total growth rates, while $n = 5, 6$ TAEs are stabilized with similar total damping rates. The trend of decreasing drive with n is at least consistent for $n = 3$–5 modes, although of course $n = 5$ is *unstable* in experiment (see Fig. 2). Additionally, the $n = 2$ TAE is stable at $t = 9.9$ s in experiment, not strongly driven. These are currently unresolved discrepancies. That said, the net damping rate $\gamma/\omega_0 \approx -2.9\%$ for the $n = 6$ TAE agrees within experimental uncertainties.

4. Hybrid kinetic-MHD simulations with MEGA

Despite NOVA-K modeling successfully reproducing many of the characteristics of the observed TAEs (such as mode frequency and radial location), the simulations of the previous section predicted an unstable $n = 2$ TAE at $t = 9.9$ s, while such a mode is not detected by any fluctuation diagnostic at that time. On the other hand, large radiative and continuum damping are predicted for the $n = 5$ mode, thus stabilizing it, yet the TAE is clearly observed in experiment.

To further investigate these features and resolve these discrepancies, a more advanced hybrid kinetic-MHD code MEGA [19] is employed. MEGA self-consistently solves the evolution of a nonlinear, resistive, full-MHD background and the dynamics of the FI population. The FIs are simulated using gyro-kinetic markers that include finite Larmor radius effects. Both the fluid plasma and FIs are coupled together by means of including the FI current density term in the MHD momentum equation applied in the particle-in-cell algorithm. The model for the thermal plasma is derived by Hazeltine and Meiss in [37], and its implementation includes diamagnetic drifts and plasma rotation, providing good accuracy of the simulated TAE frequency.

As with the NOVA-K simulations described in the previous section, the electron temperature, plasma rotation, and ion density profiles used in these simulations are taken from TRANSP (see Fig. 1). As mentioned, the density profile is corrected to account for the ^{3}He concentration, which will affect the simulated mode frequency. For these simulations, the cylindrical grid used to solve the MHD equations has a resolution of $N_R \times N_\phi \times N_Z = 128 \times 192 \times 128$; this resolution in the poloidal plane has good convergence and has been used previously to investigate harmonics $m > 10$ [38]. All modes above $n = 6$ are filtered out, so a minimum of 32 grid points in the toroidal direction per harmonic is ensured. The simulation time step is 4% of a gyro-period of a deuterium ion at the magnetic axis. For the dissipative parameters (resistivity η, viscosity ν, and diffusivity χ), normalized values $\eta/\mu_0 = \nu = \chi = 5 \times 10^{-7} v_A R_0$ are used, where v_A is the Alfvén velocity at the magnetic axis and R_0 is the major radius.

Approximately 6.2 million markers ($\sim$2 per simulation grid point) are employed to resolve the FI population using the δf method. A quasi-analytical*, anisotropic, single slowing-down distribution is used, where the maximum energy is set at $E_{\max} = 2$ MeV and the critical velocity v_c is radially dependent on $T_e(r)$. In order to match the ICRH absorption layer with the turning point of the trapped FIs, the normalized pitch of the simulated FI distribution is centered at $\Lambda = \mu B_0/E = 0.8$, with a width of $\Delta\Lambda = 0.3$, producing a real-space-integrated velocity space similar to that depicted in Fig. 4b.

A simulation is performed where the different harmonics grow linearly together and then saturate. Figure 6(a) shows the poloidal projection of the radial velocity perturbation associated with the $n = 4$ instability. The toroidal harmonics $n = 3$–5 are found to

* In MEGA, markers are uniformly distributed in real and velocity space, with weightings based on energy, normalized pitch angle, and poloidal flux.

be unstable, in agreement with the experiment. The poloidal harmonics of each toroidal harmonic are depicted in Fig. 6(b), and good agreement is seen when comparing to the mode structures from NOVA-K in Fig. 5. The locations of these harmonics are also consistent with the observed locations in this and previous experiments.

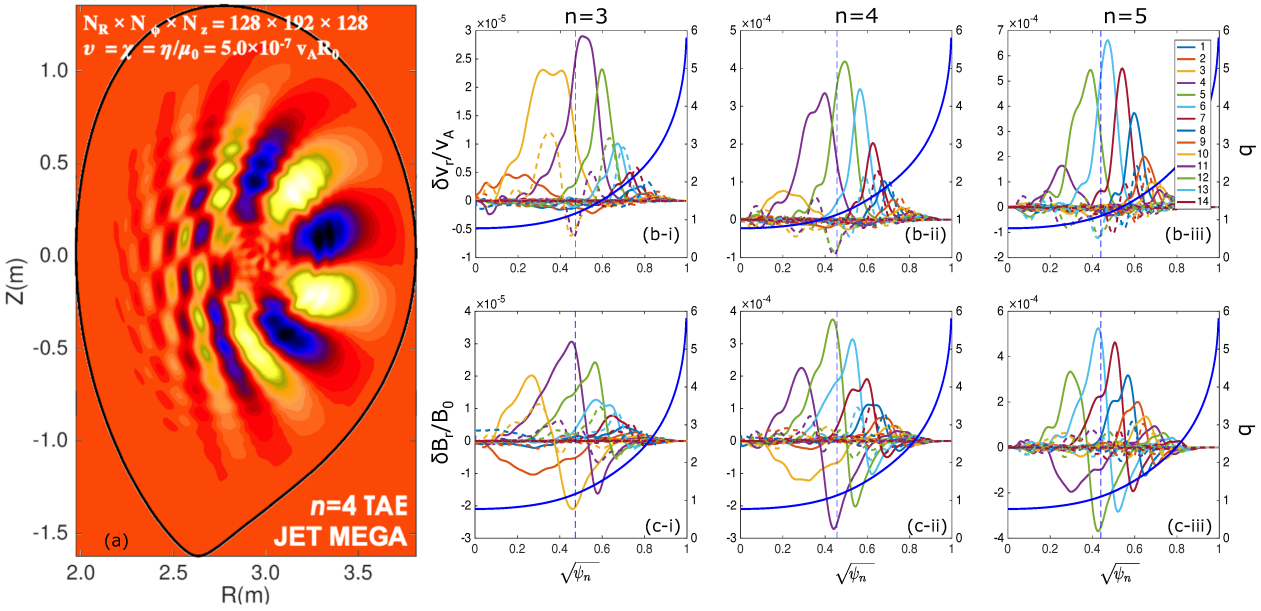

Figure 6: (a) MEGA-simulated poloidal structure of the radial velocity perturbation of the unstable $n = 4$ TAE. Radial profiles of the (b) radial velocity and (c) magnetic field perturbation for the unstable $n = 3$–5 modes, with the q-profile overlaid and surface $q = (n + 1/2)/n$ marked.

Next, another simulation is performed with twice the FI pressure from TRANSP, i.e. $2\beta_{\rm fi}$, aiming to observe the toroidal harmonics that remained stable in the previous simulation. The evolution of these fields are Fourier decomposed and plotted together with Alfvén continua in Fig. 7; frequencies are provided in Table 2. The modes $n = 3 - 6$, as expected, can be classified as TAEs since they are located within the continuum gap calculated by the ALCON code [39]. The frequency of the ALCON 1-D estimation of the Alfvén continuum for each harmonic is Doppler-shifted by the experimentally measured toroidal rotation included in the simulation. One can observe that the $n = 2$ instability strongly intersects the Alfvén continuum; thus, this mode can be classified as an energetic particle mode (EPM) at the time of interest. However, this does not mean that the unstable $n = 2$ mode observed experimentally earlier in time (see Fig. 2, $t \approx 7.5 - 9$ s) is also an EPM.

Comparing Fig. 2 and Tables 1 and 2, we see that MEGA's predicted mode frequencies are too low compared to experimental values for $n = 2$–4, but closer than NOVA-K for $n = 5, 6$. In addition, it is interesting that MEGA does not find an $n = 2$ TAE in the gap indicated by ALCON (see Fig. 7) around ∼180 kHz, while the EPM is destabilized instead.

Since MEGA reproduces the TAEs satisfactorily and finds $n = 3$–5 unstable as in the experiment, a scan in $\beta_{\rm fi}$ is performed to further investigate the intrinsic damping associated

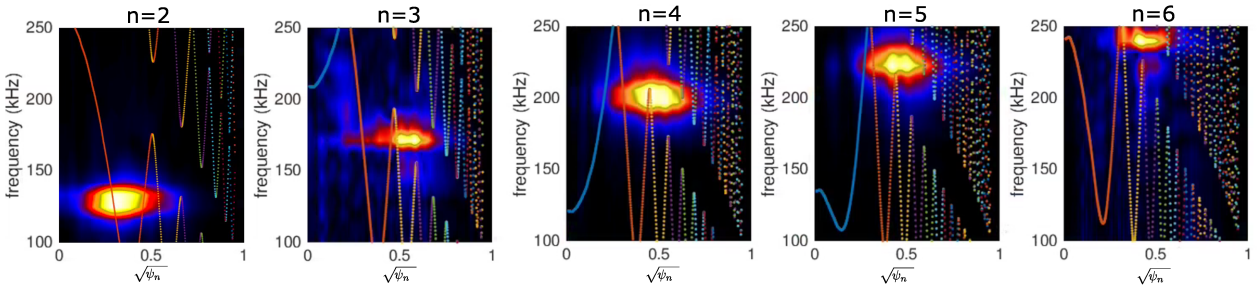

Figure 7: Fourier-decomposed radial velocity from MEGA together with the Alfvén continuum calculated by the ALCON code [39]. The modes are located within the TAE gap, except the $n = 2$ EPM.

with each mode and how sensitive the FI drive is to the applied FI pressure. To disentangle these effects for each TAE, single-n runs are performed, simulating only a fraction of the toroidal angle $\phi \in [0, 2\pi/n]$. The toroidal resolution is reduced to $N_\phi = 32$ for these runs. Seven values of $\beta_{\rm fi}$ are simulated, ranging from the value inferred from TRANSP up to $2.25\beta_{\rm fi}$. Figure 8(a) shows the temporal evolution of the energy of the $n = 3$ TAE for these different values of FI pressure, while Fig. 8(b) shows the temporal evolution of the different toroidal harmonics simulated for the case with $2\beta_{\rm fi}$.

The growth rate of the instability of each simulation is evaluated during the linear phase and plotted in Fig. 8(c) as a function of the FI pressure; specific values are also given in Table 2. Note that $n = 2$ and 6 are only observed for simulations with pressures $\geq 1.75\beta_{\rm fi}$ because those modes remain stable for lower values. A linear fit is performed to the growth rates of each toroidal mode number. The crossing point with the ordinate ($\beta_{\rm fi} = 0$) indicates the negative growth rate of the instability in the case without FIs, thereby indirectly estimating the total, or "intrinsic," mode damping.

Table 2: Total growth rates (%, damping < 0) calculated from MEGA for different values of the fast ion pressure $\beta_{\rm fi}$ from TRANSP.

Toroidal mode number (n)	2	3	4	5	6
Frequency (kHz, lab frame)	125	170	200	230	240
Fast ion beta	Total growth rates γ/ω_0 (%)				
$0.0\beta_{\rm fi}$	-17.9 ± 0.9	-6.9 ± 0.4	-8.0 ± 0.6	-8.9 ± 0.4	-4.7 ± 1.0
$0.7\beta_{\rm fi}$	-7.5 ± 1.0	2.3 ± 0.5	1.7 ± 0.7	0.1 ± 0.5	-1.2 ± 1.1
$1.0\beta_{\rm fi}$	-3.0 ± 1.0	6.2 ± 0.5	5.9 ± 0.7	3.7 ± 0.5	0.3 ± 1.1

It is interesting, although perhaps expected, that the $n = 3$–6 TAEs have similar values of the intrinsic damping, i.e. $-\gamma/\omega_0 \approx 5\%$–$10\%$, while $n = 2$ EPM is almost twice as large. In view of these computational results, one could argue that $n = 2$ and 6 modes are stable in the experiment but for different reasons: the $n = 2$ EPM has a larger intrinsic damping due to the strong interaction with the SAW continuum, while the $n = 6$ TAE has a lower FI

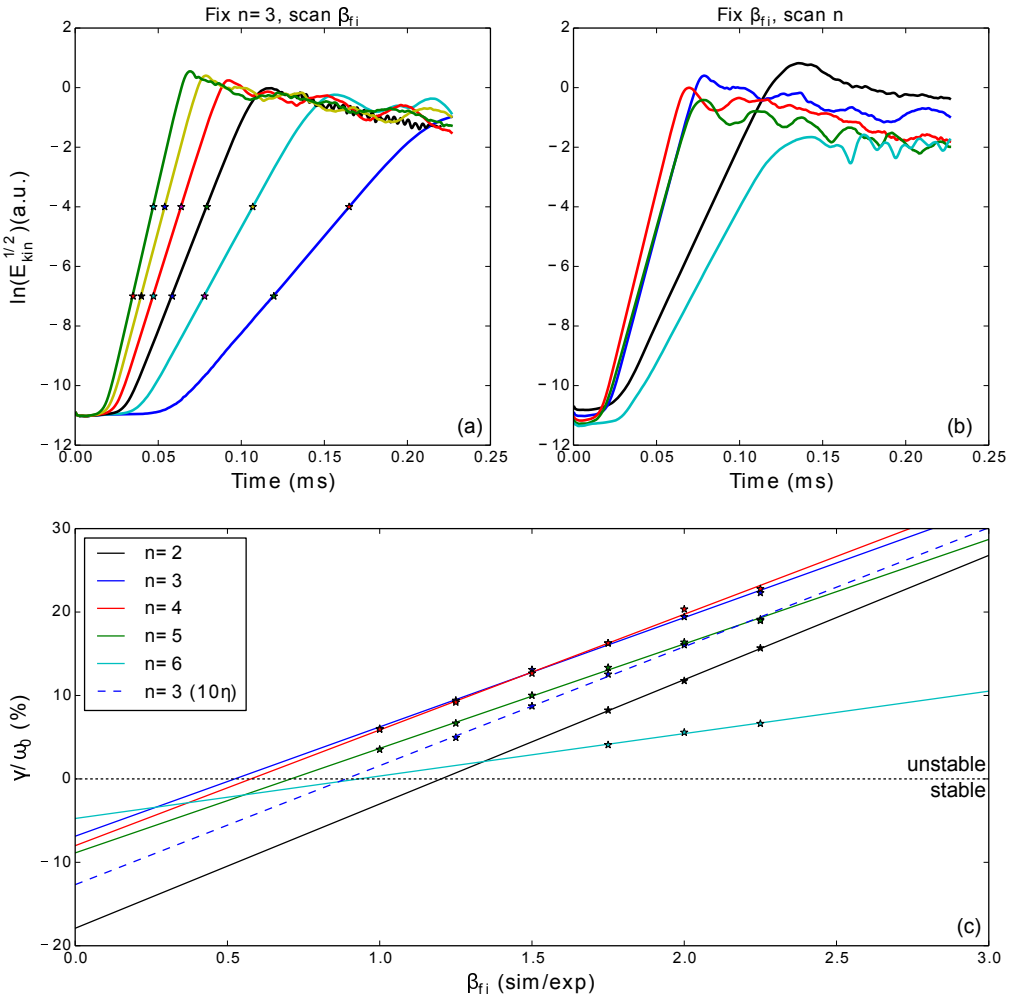

Figure 8: (a) Temporal evolution of the $n = 3$ TAE energy for different values of FI pressure $\beta_{\rm fi}$ in MEGA. (b) Temporal evolution of different toroidal harmonics for $2\beta_{\rm fi}$. (c) Growth rates as a function of $\beta_{\rm fi}$: $n = 3{-}6$ have similar values of inferred damping (at $\beta_{\rm fi} = 0$) while $n = 2$ has the largest. The slope of $n = 6$ is lower, indicating that the mode is stable due to poor FI drive. The stability of an $n = 3$ TAE with increased resistivity (10η) is also included (dashed), producing a line almost parallel to the reference $n = 3$ case, indicating that the resistivity primarily affects the mode damping, not drive.

drive, which is reflected by the lower slope in Fig. 8(c). This is only partially found in the NOVA-K results (see Table 1): The total intrinsic damping is predicted to increase with n, in disagreement with MEGA. On the other hand, the drive of the $n = 2{-}4$ modes is about twice that of the $n = 6$ mode, in agreement with MEGA, although the same applies to $n = 5$, which is a discrepancy. Moreover, there is a factor of 1-10 difference in the intrinsic damping values predicted by NOVA-K and MEGA, but part of this may be due to the resistivity used in MEGA, discussed further below.

At the experimental value of $\beta_{\rm fi}$, the $n = 3{-}5$ TAEs are unstable and decreasing in their growth rates. This qualitatively agrees with decreasing (saturated) mode amplitudes

observed by the magnetic probes in experiment (see Fig. 2). The $n = 2$ mode is heavily damped around $\sim\beta_{\rm fi}$, also in agreement with experiment. At the TRANSP value of $\beta_{\rm fi}$, the linear extrapolation of the $n = 6$ TAE growth rate would suggest a marginally *unstable* mode with $\gamma/\omega_0 \approx +0.3\%$, although the uncertainty is significant $\sim$1% (see Table 2). To best match the measured net damping rate of $-\gamma/\omega_0 \approx 2\% \pm 1\%$, we would need to decrease the FI pressure to $\sim 0.7\beta_{\rm fi}$, at which point the $n = 5$ TAE would be only marginally unstable, also in better agreement with experiment.

It is important to note that the validity of the estimated mode damping depends on the resistivity η used in these simulations; however, a value larger than the Spitzer value was chosen to accommodate MEGA's high-resolution grid [40]. To test the sensitivity to η, the $\beta_{\rm fi}$ scan was run again for the $n = 3$ harmonic using a resistivity ten times larger. The resulting growth rates are shown in Fig. 8(c). As expected, the inferred damping rate has increased by $\sim$50%, but not enough to exceed the damping estimated for the $n = 2$ EPM. The slope of the (dashed) line is very similar to the reference case, suggesting that η has little effect on the FI drive. In reality, using the true (lower) resistivity would *decrease* the net damping. Thus, while variations of η might slightly change the inferred damping, the conclusion that the $n = 2$ mode remains stable due to larger intrinsic damping and $n = 6$ due to lower FI drive is still valid.

5. Summary

In this work, we presented novel measurements of both unstable and stable TAEs observed simultaneously in a JET deuterium plasma, with steady-state parameters $B_0 = 3.7$ T, $I_{\rm p} = 2.5$ MA, $n_{\rm e0} = 6 \times 10^{19}$ m^{-3}, and $T_{\rm e0} = 5.5{-}7$ keV (see Fig. 1). The three-ion-heating scheme (D-DNBI-27% ^{3}He) was used in this discharge to accelerate $\sim$100 keV NBI-deuterons to $\sim$MeV energies (see Fig. 4) with a dominant pitch $v_\parallel/v \approx 0.5$. This fast ion (FI) population destabilized $n = 2{-}5$ TAEs, and their saturated mode amplitudes decreased with toroidal mode number n (see Fig. 2), from which decreasing FI drive was inferred. Synchronously, JET's in-vessel Alfvén Eigenmode Active Diagnostic (AEAD) resonantly excited a stable AE with normalized damping rate $-\gamma/\omega_0 \approx 2\% \pm 1\%$ (see Fig. 3). Its Doppler-shifted frequency, $f_0 \approx 245$ kHz, indicated that it was likely an $n = 6$ TAE.

Simulations with two hybrid kinetic-MHD codes, NOVA-K and MEGA, both identified AEs with similar eigenfrequencies, poloidal mode structures, and radial locations as those observed in experiment. NOVA-K's calculation of AE stability demonstrated good agreement with the $n = 3$, 4, and 6 TAEs (see Fig. 5), matching the experimentally measured damping rate of the $n = 6$ mode within uncertainties and identifying radiative damping as the dominant mechanism (see Table 1). However, there were two major discrepancies between NOVA-K and experiment: the stable $n = 2$ TAE, i.e. not seen in fluctuation data, was predicted by NOVA-K to be strongly driven, while the marginally unstable $n = 5$ TAE was predicted to be strongly damped.

Improved agreement was then obtained with MEGA for all modes: the unstable $n = 3{-}5$

and stable $n = 2, 6$ modes (see Figs. 6 and 7). By scanning the FI pressure β_{fi} in MEGA, an $n = 2$ EPM and $n = 6$ TAE were destabilized and identified. The intrinsic damping was extrapolated to $\beta_{\text{fi}} = 0$ (see Fig. 8 and Table 2), and the $n = 2, 6$ modes were found to be stabilized for two different reasons: the former EPM by higher intrinsic damping due to strong interaction with the Alfvén continuum, and the latter TAE by lower fast ion drive. Yet the best agreement of the MEGA growth rates with experiment was not found at the value of β_{fi} inferred from TRANSP, but rather at $\sim 0.7\beta_{\text{fi}}$.

These disagreements between experiment and simulation still need to be resolved. One resolution could be found by manipulating the various inputs within experimental error bars, and that exploration is left for future work. The codes also include different physics (see [8] and others for further details): NOVA-K is a perturbative eigenvalue code with some contributions to the linear growth/damping rate calculated analytically, whereas MEGA is a first-principle, resistive, fully nonlinear initial value code. The benefit of NOVA-K is the identification of various drive and damping mechanisms and their uncertainties, whereas MEGA gives only the total - though perhaps more accurate - growth rate.

The codes may also need to improve their stability calculations of intrinsic damping and drive. These data, as well as large databases of stable AEs (see [5, 10, 11] and references therein), could help guide this effort. Nevertheless, the trends of decreasing growth rate for $n = 3{-}6$ TAEs in both MEGA and NOVA-K is promising, and so is the relatively good match with the experimentally measured damping rate. Preliminary results from the orbit-following code ORBIT [41] indicate some strong interactions of the TAEs with trapped fast ions, and this should be looked into further. Additional upcoming work will include similar analyses of AE stability in DT plasmas from the recent JET 2021 campaign, during which the AEAD actively excited over 2000 stable AEs.

Looking toward future tokamaks, like ITER and SPARC, a similar modeling strategy could be used to predict and optimize AE stability: Multiple codes, e.g. NOVA-K and MEGA, should be used to identify AEs (and other FI-driven modes), and a cross-check performed among them to confirm similar mode frequencies, structures, locations, etc. The findings of this work suggest that scanning the FI pressure $\pm 30\%$ may be required (at least in MEGA) to best match reality, although $+30\%$ may be too conservative and uncertainties must be considered. Both the MEGA β_{fi}-scan and NOVA-K breakdown can then identify the dominant contributions to damping and drive, and various parameters could be tuned to help stabilize those modes, e.g. plasma elongation or ICRH resonance location.

Acknowledgments

The authors are grateful to the reviewers whose comments improved this paper. The authors also thank P. Bonofiglo, N. Dreval, N. Gorelenkov, W.W. Heidbrink, and Y. Todo for fruitful discussions. This work was supported by US DOE grants DE-SC0014264, DE-AC02-09CH11466, DE-SC0020412, and DE-SC0020337, as well as the Brazilian agency FAPESP Project 2011/50773-0. This work has been carried out within the framework of

the EUROfusion Consortium, funded by the European Union via the Euratom Research and Training Programme (Grant Agreement No 101052200 – EUROfusion). Views and opinions expressed are however those of the author(s) only and do not necessarily reflect those of the European Union or the European Commission. Neither the European Union nor the European Commission can be held responsible for them. This research used resources of the National Energy Research Scientific Computing Center (NERSC), a U.S. Department of Energy Office of Science User Facility located at Lawrence Berkeley National Laboratory, operated under Contract No. DE-AC02-05CH11231 using NERSC award FES-ERCAP20598.

References

[1] A. Fasoli, C. Gormenzano, H. L. Berk, B. Breizman, S. Briguglio, D. S. Darrow, N. Gorelenkov, W. W. Heidbrink, A. Jaun, S. V. Konovalov, R. Nazikian, J. M. Noterdaeme, S. Sharapov, K. Shinohara, D. Testa, K. Tobita, Y. Todo, G. Vlad, and F. Zonca. Chapter 5: Physics of energetic ions. *Nuclear Fusion*, 47(S264–S284):S264–S284, 2007.

[2] A. Fasoli, D. Borba, G. Bosia, D. J. Campbell, J. A. Dobbing, C. Gormezano, J. Jacquinot, P. Lavanchy, J. B. Lister, P. Marmillod, J. M. Moret, A. Santagiustina, and S. Sharapov. Direct measurement of the damping of toroidicity-induced Alfvén eigenmodes. *Physical Review Letters*, 75(4):645–648, 1995.

[3] T. Panis, D. Testa, A. Fasoli, A. Klein, H. Carfantan, P. Blanchard, and JET-EFDA Contributors. Optimization of the active MHD spectroscopy system on JET for the excitation of individual intermediate and high-n Alfvén eigenmodes. *Nuclear Fusion*, 50(084019), 2010.

[4] P. Puglia, W. Pires de Sa, P. Blanchard, S. Dorling, S. Dowson, A. Fasoli, J. Figueiredo, R. Galvão, M. Graham, G. Jones, C. Perez von Thun, M. Porkolab, L. Ruchko, D. Testa, P. Woskov, M.A. Albarracin-Manrique, and JET Contributors. The upgraded JET toroidal Alfvén eigenmode diagnostic system. *Nuclear Fusion*, 56(11):112020, nov 2016.

[5] R A Tinguely, P G Puglia, N Fil, S Dowson, M Porkolab, A Fasoli, D Testa, and Jet Contributors. Results from the Alfvén Eigenmode Active Diagnostic during the 2019- 2020 JET deuterium campaign. *Plasma Phys. Control. Fusion*, 62:11, 2020.

[6] King-Lap Wong. A review of Alfvén eigenmode observations in toroidal plasmas. *Plasma Physics and Controlled Fusion*, 41(1):R1–R56, jan 1999.

[7] W. W. Heidbrink. Basic physics of Alfvén instabilities driven by energetic particles in toroidally confined plasmas. *Physics of Plasmas*, 15(5):055501, may 2008.

[8] S. Taimourzadeh, E.M. Bass, Y. Chen, C. Collins, N.N. Gorelenkov, A. Könies, Z.X. Lu, D.A. Spong, Y. Todo, M.E. Austin, J. Bao, A. Biancalani, M. Borchardt, A. Bottino, W.W. Heidbrink, R. Kleiber, Z. Lin, A. Mishchenko, L. Shi, J. Varela, R.E. Waltz, G. Yu, W.L. Zhang, and Y. Zhu. Verification and validation of integrated simulation of energetic particles in fusion plasmas. *Nuclear Fusion*, 59(6):066006, apr 2019.

[9] D. Borba, A. Fasoli, N.N. Gorelenkov, S. Gunter, Ph. Lauber, N. Mellet, R. Nazikian, T. Panis, S.D. Pinches, D. Spong, D. Testa, and JET-EFDA Contributors. The Influence of Plasma Shaping on the Damping of Toroidal Alfvén Eigenmodes. *23rd IAEA Fusion Energy Conference*, (THW/P7-08):1–8, 2010.

[10] R A Tinguely, P G Puglia, N Fil, S Dowson, M Porkolab, A Dvornova, A Fasoli, M Fitzgerald, V Guillemot, G T A Huysmans, M Maslov, S Sharapov, and D Testa. Experimental studies of plasma-antenna coupling with the JET Alfvén Eigenmode Active Diagnostic. *Nuclear Fusion*, 61:26003–26017, 2021.

[11] R.A. Tinguely, N. Fil, P.G. Puglia, S. Dowson, M. Porkolab, V. Guillemot, M. Podestà, M. Baruzzo,

R. Dumont, A. Fasoli, M. Fitzgerald, Ye.O. Kazakov, M.F.F. Nave, M. Nocente, J. Ongena, S.E. Sharapov, Ž. Štancar, and JET Contributors. A novel measurement of marginal alfvén eigenmode stability during high power auxiliary heating in JET. *Nuclear Fusion*, 62(7):076001, apr 2022.

[12] J. A. Snipes, D. Schmittdiel, A. Fasoli, R. S. Granetz, and R. R. Parker. Initial active MHD spectroscopy experiments exciting stable Alfvén eigenmodes in Alcator C-Mod. *Plasma Physics and Controlled Fusion*, 46(4):611–620, apr 2004.

[13] J. A. Snipes, N. Basse, C. Boswell, E. Edlund, A. Fasoli, N. N. Gorelenkov, R. S. Granetz, L. Lin, Y. Lin, R. Parker, M. Porkolab, J. Sears, S. Sharapov, V. Tang, and S. Wukitch. Active and fast particle driven alfvén eigenmodes in alcator c-mod. *Physics of Plasmas*, 12(5):056102, 2005.

[14] J. A. Snipes, N. N. Gorelenkov, and J. A. Sears. A comparison of measured and calculated toroidal Alfvén eigenmode damping rates in Alcator C-Mod. *Nuclear Fusion*, 46(12):1036–1046, dec 2006.

[15] Joelle Mailloux. Overview of jet results for optimising iter operation. *Nuclear Fusion*, 2022.

[16] CZ Cheng. Kinetic extensions of magnetohydrodynamics for axisymmetric toroidal plasmas. *Physics Reports*, 211(1):1–51, 1992.

[17] GY Fu and CZ Cheng. Excitation of high-n toroidicity-induced shear Alfvén eigenmodes by energetic particles and fusion alpha particles in tokamaks. *Physics of Fluids B: Plasma Physics*, 4(11):3722–3734, 1992.

[18] NN Gorelenkov, Chio-Zong Cheng, and GY Fu. Fast particle finite orbit width and Larmor radius effects on low-n toroidicity induced Alfvén eigenmode excitation. *Physics of Plasmas*, 6(7):2802–2807, 1999.

[19] Y. Todo and T. Sato. Linear and nonlinear particle-magnetohydrodynamic simulations of the toroidal Alfvén eigenmode. *Physics of Plasmas*, 5:1321–1327, 1998.

[20] Ye O Kazakov, Massimo Nocente, MJ Mantsinen, Jozef Ongena, Yuriy Baranov, Teddy Craciunescu, Mykola Dreval, Remi Dumont, Jacob Eriksson, Jeronimo Garcia, et al. Plasma heating and generation of energetic D ions with the 3-ion ICRF+ NBI scenario in mixed HD plasmas at JET-ILW. *Nuclear Fusion*, 60(11):112013, 2020.

[21] Ye. O. Kazakov, J. Ongena, J. C. Wright, S. J. Wukitch, V. Bobkov, J. Garcia, V. G. Kiptily, M. J. Mantsinen, M. Nocente, M. Schneider, H. Weisen, Y. Baranov, M. Baruzzo, R. Bilato, A. Chomiczewska, R. Coelho, T. Craciunescu, K. Crombé, M. Dreval, R. Dumont, P. Dumortier, F. Durodié, J. Eriksson, M. Fitzgerald, J. Galdon-Quiroga, D. Gallart, M. Garcia-Muñoz, L. Giacomelli, C. Giroud, J. Gonzalez-Martin, A. Hakola, P. Jacquet, T. Johnson, A. Kappatou, D. Keeling, D. King, K. K. Kirov, P. Lamalle, M. Lennholm, E. Lerche, M. Maslov, S. Mazzi, S. Menmuir, I. Monakhov, F. Nabais, M. F. F. Nave, R. Ochoukov, A. R. Polevoi, S. D. Pinches, U. Plank, D. Rigamonti, M. Salewski, P. A. Schneider, S. E. Sharapov, Ž. Štancar, A. Thorman, D. Valcarcel, D. Van Eester, M. Van Schoor, J. Varje, M. Weiland, and N. Wendler. Physics and applications of three-ion icrf scenarios for fusion research. *Physics of Plasmas*, 28(2):020501, 2021.

[22] L.L. Lao, H. St. John, R.D. Stambaugh, A.G. Kellman, and W. Pfeiffer. Reconstruction of current profile parameters and plasma shapes in tokamaks. *Nuclear Fusion*, 25(11):1611–1622, 1985.

[23] Joshua Breslau, Marina Gorelenkova, Francesca Poli, Jai Sachdev, and Xingqiu Yuan. TRANSP. [Computer Software] https://doi.org/10.11578/dc.20180627.4, jun 2018.

[24] RJ Hawryluk. An empirical approach to tokamak transport. In Coppi et al, editor, *Physics Close to Thermonuclear Conditions, Ed. B*, volume 19. Brussels: Commission of the European Communities, Brussels, 1980.

[25] JPHE Ongena, I Voitsekhovitch, M Evrard, and D McCune. Numerical transport codes. *Fusion Science and Technology*, 61(2T):180–189, 2012.

[26] Mykola Dreval, Sergei E Sharapov, Yevgen Kazakov, Jozef Ongena, Massimo Nocente, Rui Calado, Rui Coelho, Jorge Ferreira, Antonio C A Figueiredo, Michael Fitzgerald, Jeronimo Garcia, Carine Giroud, Nicholas Hawkes, Vasily Kiptily, Fernando Nabais, Maria Filomena Ferreira Nave, Henri Weisen, Teddy Craciunescu, Mirko Salewski, and Ziga Stancar. Alfvén cascade eigenmodes above the tae-frequency and localization of alfvén modes in d- 3 he plasmas on jet. *Nuclear Fusion*, 2021.

[27] Alexei Pankin, Douglas McCune, Robert Andre, Glenn Bateman, and Arnold Kritz. The tokamak

monte carlo fast ion module nubeam in the national transport code collaboration library. *Computer Physics Communications*, 159(3):157–184, 2004.

[28] M Brambilla. Numerical simulation of ion cyclotron waves in tokamak plasmas. *Plasma Physics and Controlled Fusion*, 41(1):1–34, jan 1999.

[29] M.A. Van Zeeland, W.W. Heidbrink, S.E. Sharapov, D. Spong, A. Cappa, Xi Chen, C. Collins, M. García-Muñoz, N.N. Gorelenkov, G.J. Kramer, P. Lauber, Z. Lin, and C. Petty. Electron cyclotron heating can drastically alter reversed shear Alfvén eigenmode activity in DIII-D through finite pressure effects. *Nuclear Fusion*, 56(11):112007, jul 2016.

[30] F. Nabais, V. Aslanyan, D. Borba, R. Coelho, R. Dumont, J. Ferreira, A. Figueiredo, M. Fitzgerald, E. Lerche, J. Mailloux, M. Mantsinen, P. Rodrigues, M. Porkolab, P. Puglia, S.E. Sharapov, and JET Contributors. TAE stability calculations compared to TAE antenna results in JET. *Nuclear Fusion*, 58(8):082007, aug 2018.

[31] V. Aslanyan, S. Taimourzadeh, L. Shi, Z. Lin, G. Dong, P. Puglia, M. Porkolab, R. Dumont, S. E. Sharapov, J. Mailloux, M. Tsalas, M. Maslov, A. Whitehead, R. Scannell, S. Gerasimov, S. Dorling, S. Dowson, H. K. Sheikh, T. Blackman, G. Jones, A. Goodyear, K. K. Kirov, P. Blanchard, A. Fasoli, and D. Testa. Gyrokinetic simulations of toroidal Alfvén eigenmodes excited by energetic ions and external antennas on the Joint European Torus. *Nuclear Fusion*, 59(2), feb 2019.

[32] H. L. Berk, R. R. Mett, and D. M. Lindberg. Arbitrary mode number boundary-layer theory for nonideal toroidal Alfvén modes. *Physics of Fluids B*, 5(11):3969–3996, nov 1993.

[33] G. Y. Fu, C. Z. Cheng, R. Budny, Z. Chang, D. S. Darrow, E. Fredrickson, E. Mazzucato, R. Nazikian, K. L. Wong, and S. Zweben. Analysis of alpha particle-driven toroidal Alfvén eigenmodes in Tokamak Fusion Test Reactor deuterium-tritium experiments. *Physics of Plasmas*, 3(11):4036–4045, nov 1996.

[34] R. R. Mett and S. M. Mahajan. Kinetic theory of toroidicity-induced Alfvén eigenmodes. *Physics of Fluids B*, 4(9):2885–2893, sep 1992.

[35] G. W. Bowden, A. Könies, M. J. Hole, N. N. Gorelenkov, and G. R. Dennis. Comparison of methods for numerical calculation of continuum damping. *Physics of Plasmas*, 21(5):052508, 2014.

[36] D Borba, B Alper, R.V Budny, A Fasoli, R.F Heeter, W Kerner, S.E Sharapov, and P Smeulders. Beam driven alfvén eigenmodes and fishbones in JET. *Nuclear Fusion*, 40(4):775–783, apr 2000.

[37] R. D. Hazeltine and J. D. Meiss. Shear-Alfvén dynamics of toroidally confined plasmas. *Physics Reports*, 121:1–164, 5 1985.

[38] Y Todo, M Sato, Hao Wang, M Idouakass, and R Seki. Magnetohydrodynamic hybrid simulation model with kinetic thermal ions and energetic particles. *Plasma Physics and Controlled Fusion*, 63(7):075018, jun 2021.

[39] W. Deng, Z. Lin, I. Holod, Z. Wang, Y. Xiao, and H. Zhang. Linear properties of reversed shear Alfvén eigenmodes in the DIII-D tokamak. *Nuclear Fusion*, 52(4), apr 2012.

[40] A. Bierwage, Y. Todo, N. Aiba, and K. Shinohara. Sensitivity study for N-NB-driven modes in JT-60U: boundary, diffusion, gyroaverage, compressibility. *Nuclear Fusion*, 56:106009, 8 2016.

[41] R. B. White and M. S. Chance. Hamiltonian guiding center drift orbit calculation for plasmas of arbitrary cross section. *The Physics of Fluids*, 27(10):2455–2467, 1984.